Fold-pitchfork bifurcation for maps with Z_2 symmetry in pipe flow

F. Marques,* F. Mellibovsky, and A. Meseguer
Departament de Física Aplicada, Universitat Politècnica de Catalunya, C/ Jordi Girona Salgado s/n, Mòdul B5 Campus Nord, 08034 Barcelona, Spain
(Received 18 December 2012; published 11 July 2013)

This study aims to provide a better understanding of recently identified transition scenarios exhibited by traveling wave solutions in pipe flow. This particular family of solutions are invariant under certain reflectional symmetry transformations and they emerge from saddle-node bifurcations within a two-dimensional parameter space characterized by the length of the pipe and the Reynolds number. The present work precisely provides a detailed analysis of a codimension-two saddle-node bifurcation arising in discrete dynamical systems (maps) with $\mathbb{Z}_2$ symmetry. Normal form standard techniques are applied in order to obtain the reduced map up to cubic order. All possible bifurcation scenarios exhibited by this normal form are analyzed in detail. Finally, a qualitative comparison of these scenarios with the ones observed in the aforementioned hydrodynamic problem is provided.

DOI: 10.1103/PhysRevE.88.013006 PACS number(s): 47.20.Ky, 83.50.−v, 05.45.−a, 47.35.−i

I. INTRODUCTION

Equivariant normal form theory constitutes the backbone of many instability phenomena analyses in fluid dynamics [1]. Identifying codimension and symmetries of the underlying bifurcations helps simplify the study of the dynamics and predict transition scenarios of the flow under study [2]. Whereas this formal approach has been extensively applied to analyze instabilities of base flows that exhibit local bifurcations, it has rarely been used to try and understand subcritical transition to turbulence (i.e., in the absence of linear instabilities of the basic solution) such as for the flow in a pipe of circular cross section [3–5]. For this particular problem, the Hagen-Poiseuille parabolic solution is believed to be linearly stable [6] for all flow rates and to never undergo local bifurcation. However, finite amplitude perturbations are capable of triggering turbulence at moderate flow rates.

A broad variety of families of traveling wave solutions has been numerically computed during the last decade [7–10]. These exact solutions are believed to play a relevant role both during the transition process and for the intrinsic sustainment of subcritical turbulence [8,11]. The aforementioned studies have addressed qualitative analyses of these solutions within the two-dimensional (Re,κ) parameter space, where $\mathrm{Re} = UD/\nu$ is the Reynolds number based on the pipe diameter D, the average flow speed U, and the kinematic viscosity of the fluid ν, and $\lambda = 2\pi/\kappa$ is the axial wavelength in units of $D/2$. Combined computational and experimental efforts have recently identified traveling wave solutions in pipe flow transitional relaminarizing dynamics [12], thus evidencing the potential relevance of these families of secondary solutions for turbulence.

Different attempts have been made in order to provide an explanation for the eventual development of turbulent dynamics at sufficiently high values of the Reynolds number in this and other subcritical shear flows. Some of the traveling wave solutions have been shown to exhibit bifurcations that generate relative periodic orbits [13] or modulated traveling waves, thus initiating a supercritical cascade towards higher complexity that would eventually lead to chaos and turbulence. Recent computations [14] reported that at least one family of twofold azimuthally periodic traveling waves undergoes a supercritical bifurcation cascade that leads to time-chaotic dynamics. When parametrized in terms of (Re,κ), the traveling wave family at the origin of the bifurcation cascade appears in a codimension-two Takens-Bogdanov bifurcation [15]. These waves exhibit a shift-reflect symmetry (they are invariant when shifted half a wavelength downstream and then reflected with respect to a diametral plane) that is broken along the bifurcation cascade producing an array of spiraling secondary flows that only exist within a limited range of λ and Re. The sequence of local bifurcations, with two competing modes, one related to a Hopf and the other to the breach of the shift-reflect symmetry in a pitchfork bifurcation, combined with the role the symmetry seems to play in the final chaos-inducing global bifurcation. In Ref. [14] it was suggested that the dynamics observed might be explained through the study of a codimension-two bifurcation of the Poincaré map associated with the periodic orbit emerging from the Hopf bifurcation. In this study we confirm that this is the case, combining extensive new numerical simulations around the codimension-two point, and analyzing the bifurcation using dynamical systems theory. The relevant bifurcation is a fold-pitchfork bifurcation for maps with Z_2 symmetry, corresponding to the shift-reflect aforementioned symmetry. This bifurcation had not been studied in detail previously, and in Sec. II we present a detailed analysis of the different scenarios of this bifurcation, closely following the recent analysis of the fold-flip bifurcation by Ref. [16], which bears strong similarities with the present problem. In Sec. III we conduct extensive numerical simulations in the pipe flow problem that shows the relevance of the fold-pitchfork bifurcation for maps in the understanding of the bifurcation cascade that leads to chaos and turbulence.

II. NORMAL FORM FOR THE FOLD-PITCHFORK BIFURCATION

Assume we have a map with a fixed point that has two $+1$ eigenvalues for given parameter values, that the system has a symmetry group Z_2, i.e., there exists a symmetry operation S such that $S^2 = I$ is the identity, and that this symmetry acts

*francisco.marques@upc.edu

differently on the two eigenvectors corresponding to the two $+1$ critical eigenvalues. This means that the action of S leaves invariant one of the eigenvalues, while the other eigenvalue changes sign. The center manifold is two dimensional, and the map is of the form

$$x \to f(x,\alpha) = Lx + P(x,\alpha). \tag{1}$$

where $x = (x_1,x_2) \in \mathbb{R}^2$, L is the linear part of the map, P is the nonlinear part and α are parameters. The normal form of the map can be chosen so that P satisfies [17]

$$P(L^\dagger x,\alpha) = L^\dagger P(x,\alpha), \quad P(Sx,\alpha) = SP(x,\alpha), \tag{2}$$

where $L^\dagger$ is the adjoint of L. In the absence of symmetry the double $+1$ eigenvalue corresponds to the 1:1 strong resonance [18], with a linear part of the form

$$L_{1:1} = \begin{pmatrix} 1 & 1 \\ 0 & 1 \end{pmatrix}. \tag{3}$$

The presence of the symmetry strongly modifies the normal form. The equivariance of the map under S implies that S commutes with L. This fact and the assumed action of S on the eigenvectors results in

$$S = \begin{pmatrix} 1 & 0 \\ 0 & -1 \end{pmatrix}, \quad L = \begin{pmatrix} 1 & 0 \\ 0 & 1 \end{pmatrix}, \tag{4}$$

hence L is the identity and the first equation in (2) is trivially satisfied. Let $P = [P_1(x,\alpha),P_2(x,\alpha)]$; due to the presence of the symmetry, from (2) we obtain that P_1 is an even function of x_2, and P_2 is an odd function of x_2. The normal form up to order three in x is then

$$x_1 \to f_1(x,\alpha) = \sigma + \lambda_1 x_1 + \tfrac{1}{2} g_{20} x_1^2 + \tfrac{1}{2} g_{02} x_2^2 + \tfrac{1}{6} g_{30} x_1^3 + \tfrac{1}{2} g_{12} x_1 x_2^2, \tag{5a}$$

$$x_2 \to f_2(x,\alpha) = \lambda_2 x_2 + h_{11} x_1 x_2 + \tfrac{1}{2} h_{21} x_1^2 x_2 + \tfrac{1}{6} h_{03} x_2^3, \tag{5b}$$

where all the coefficients are functions of the parameters α, and $\sigma(0) = 0$, $\lambda_1(0) = \lambda_2(0) = 1$.

The normal form (5) resembles very much the normal form of the fold-flip bifurcation, recently analyzed by Ref. [16]. The only difference is that in the fold-flip bifurcation $\lambda_2(0) = -1$. The reason for this similitude is that the linear part in the fold-flip case is identical to S in the present case, and therefore the equation satisfied by the normal form function P is the same. From another point of view, the dynamics generated by the -1 eigenvalue in the fold-flip bifurcation is replaced here by the action of the Z_2 symmetry S. Nevertheless, this change of sign results in significant differences between both problems: the eigenvalues in our case are $\{+1,+1\}$, while in the fold-flip case are $\{+1,-1\}$, so period doublings, allowed in the fold-flip case, are absent in our problem, that in addition has the extra symmetry S. The subsequent analysis presented here closely follows the analysis in Ref. [16], with the appropriate modifications due to the different sign of the eigenvalues and the presence of the symmetry.

The normal form (5) has been obtained with the standard normal form reduction: a small deformation of the identity of order k in x is used to simplify the order-k terms. However, (5) still has seven nonlinear terms. Further reduction is possible, by assuming that some of the second-order coefficients are not zero, and using a small deformation of the identity of second order in x in order to simplify the third-order terms. The simplified normal form obtained this way is called the hypernormal form [19,20]. In the present problem, assuming that $h_{11}(0) \neq 0$, it is possible to cancel out the cubic nonlinear terms in the second equation, and simplify some additional coefficients. The desired transformation is

$$y_1 = \Lambda_1(x) = \epsilon + x_1 + \tfrac{1}{2} A x_1^2 + \tfrac{1}{2} B x_2^2, \tag{6a}$$

$$y_2 = \Lambda_2(x) = x_2. \tag{6b}$$

The transformation Λ has the same parity properties as f, Λ_1 even and Λ_2 odd with respect to x_2. Therefore, the transformed map $y \to \tilde{f}(y) = \Lambda(f(x))$, where $y = \Lambda(x)$, will also have the same parity properties as the original map (5). After some computations detailed in Appendix A, we arrive at the hypernormal form for the fold-pitchfork bifurcation, truncated up to and including terms of order three

$$x_1 \to F_1(x,\mu) = \mu_1 + (1+\mu_2)x_1 + \tfrac{1}{2} a x_1^2 + \tfrac{1}{2} b x_2^2 + \tfrac{1}{6} c x_1^3 + \tfrac{1}{2} d x_1 x_2^2, \tag{7a}$$

$$x_2 \to F_2(x,\mu) = x_2 - x_1 x_2. \tag{7b}$$

This normal form depends on two small parameters μ_1 and μ_2, i.e., is a codimension-two bifurcation, and contains four constants a, b, c, and d, which in fact are functions of the parameters μ. This normal form is Z_2 equivariant by the action of S, and is identical with the normal form of the fold-flip bifurcation, except for the change of sign of the second equation [see Ref. [16], Eq. (30)]. From the form of F_2 we observe that the $x_2 = 0$ horizontal axis is an invariant curve. For $x_1 < 1$, i.e., in a neighborhood of the origin where the normal form analysis is valid, the image of a point on the upper plane $x_2 > 0$ remains on the upper plane. The half plane $x_2 > 0$ is invariant, and the trajectories on the lower half plane $x_2 < 0$ are obtained by applying the symmetry S to the ones in the upper half plane. Here horizontal, upper, and lower refer to the (x_1,x_2) phase space coordinates, as plotted in all phase portraits from Fig. 2 on.

A. Fixed points and their local bifurcations

The fixed points of the map are obtained by solving $F(x,\mu) = x$. There are two types of fixed points: those with $x_1 = 0$ and those with $x_2 = 0$. The fixed points with $x_2 = 0$ are the roots of a cubic equation, with two roots close to the origin ($\mu_1 = \mu_2 = 0$), and a third root that remains away from the origin for μ small, that will not be considered in our normal form analysis valid only for μ small. At lowest order, the two roots are

$$Q_\pm = \left(\frac{1}{a}\left(-\mu_2 \pm \sqrt{\mu_2^2 - 2a\mu_1}\right) + \text{hot},0 \right). \tag{8}$$

where hot stands for higher-order terms in μ (the details of the computations are in Appendix B). These two roots merge and disappear along a curve of fold or saddle-node bifurcations

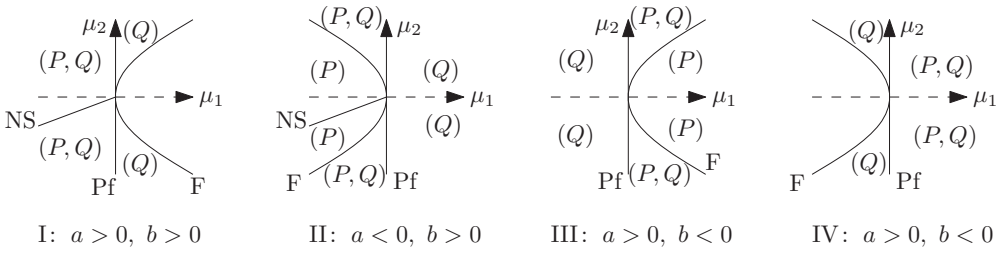

FIG. 1. Regime diagrams of the four scenarios of the fold-pitchfork bifurcation. F, Pf, and NS are the fold, pitchfork and Neimark-Sacker bifurcation curves. The fixed points that exist in the different parameter regions are indicated in brackets.

given by

$$\text{F: } 2a\mu_1 = \mu_2^2\left(1 + \frac{1}{3}\frac{c\mu_2}{a^2} + \text{hot}\right), \tag{9}$$

where we have assumed the nondegeneracy condition $a \neq 0$. $Q_\pm$ exist to the left of the parabolic type curve $2a\mu_1 = \mu_2^2 + \text{hot}$ if $a > 0$, and to the right if $a < 0$. The nature of the $Q_\pm$ points depends on sign$(a\mu_2)$. If $a\mu_2 < 0$, one of the Q points is a saddle (one stable direction and the other unstable) and the other point is stable; if $a\mu_2 > 0$, one point is a saddle and the other point is a repeller (both directions unstable). There are no additional bifurcations of $Q_\pm$ for small μ values.

There are two additional fixed points with $x_1 = 0$,

$$P_\pm = (0, \pm\sqrt{-2\mu_1/b}), \tag{10}$$

that exist only if $b\mu_1 < 0$, i.e., at one side of the straight line $\mu_1 = 0$: to the left if $b > 0$, and to the right if $b < 0$. We will assume from now on the additional nondegeneracy condition $b \neq 0$. The two new fixed points are symmetrically related: $SP_+ = P_-$. On the line $\mu_1 = 0$ both fixed points $P_\pm$ merge with one of the $Q_\pm$ points and disappear, in a pitchfork bifurcation. The symmetric fixed points $P_\pm$ undergo a Neimark-Sacker bifurcation along the curve $\mu_2 = (d/b + 2)\mu_1$, $\mu_1 \leqslant 0$; in this bifurcation an invariant circle is born around each of the fixed points $P_\pm$; the Neimark-Sacker bifurcation only takes place if $b > 0$.

In summary, we have found four different scenarios with two or three different bifurcation curves: a fold or saddle-node F, a pitchfork Pf, and a Neimark-Sacker NS. The corresponding regime diagrams in parameter space are shown in Fig. 1.

B. ODE approximating the map

The invariant circle born at the NS curve must disappear when we move around the origin in parameter space. This may happens via the formation of a heteroclinic structure involving $Q_\pm$, or via a blowup of the invariant cycle, that leaves the local neighborhood of the origin in phase space. In order to study these global bifurcation phenomena, we derive an ODE system such that the unit shift along the orbits approximates the map (7).

Given a map

$$x \to F(x,\mu) = Lx + N(x,\mu), \tag{11}$$

we want to obtain an ODE

$$\dot{x} = G(x,\mu) = \Lambda x + Y(x,\mu), \tag{12}$$

such that its flow $\phi^t(x,\mu)$ at $t = 1$ coincides with F up to a given order in (x,μ): $\phi^1(x,\mu) = F(x,\mu) + O(k)$. In order to compute $\phi^t(x,\mu)$ as a power series in (x,μ), a method based on Picard iterations, described in detail in Appendix C has been used, and the sought ODE, up to terms of $O(x^4)$, $O(x^2\mu)$, and $O(\mu^2)$ is given by

$$\dot{x}_1 = \mu_1 + \left(\mu_2 - \tfrac{1}{2}a\mu_1\right)x_1 + \tfrac{1}{2}ax_1^2 + \tfrac{1}{2}bx_2^2 + \left(\tfrac{1}{6}c - \tfrac{1}{4}a^2\right)x_1^3 + \left(\tfrac{1}{2}d + \tfrac{1}{4}(2-a)b\right)x_1x_2^2, \tag{13a}$$

$$\dot{x}_2 = \tfrac{1}{2}\mu_1 x_2 - x_1x_2 - \tfrac{1}{4}(2-a)x_1^2x_2 + \tfrac{1}{4}bx_2^3. \tag{13b}$$

This ODE is identical to the ODE discussed in Ref. [16] in the context of the fold-flip bifurcation for maps. Therefore the analysis of the ODE is identical, and we briefly summarize the main results.

C. Analysis of the ODE approximating the map

There are three curves on which equilibria of (13) undergo local bifurcations

$$\text{F: } (x_1,x_2,\mu_1) = \left(-\mu_2/a + O\left(\mu_2^2\right), 0, \mu_2^2/(2a) + O\left(\mu_2^3\right)\right), \tag{14}$$

$$\text{Pf: } (x_1,x_2,\mu_1) = (0,0,0), \tag{15}$$

$$\text{NS: } (x_1,x_2,\mu_2) = (0, \pm\sqrt{-2\mu_1/b}, (b/b+2)\mu_1), \tag{16}$$

These are the same expansions as we computed for the fold, pitchfork and Neimark-Sacker bifurcation curves for the map (7). The invariant curves born at the Neimark-Sacker bifurcation cannot exist everywhere. They should disappear through some global bifurcations.

If $a > 0$, $b > 0$ and $\mu_1 < 0$ the vector field (13) has two saddles $Q_\pm$, which are always connected by a heteroclinic orbit along the x_1 axis. There exists another heteroclinic orbit along the curve

$$\text{Het: } \mu_2 = \frac{\mu_1}{3+a}\left(\frac{1}{b}(a+2)(d+2b) + \frac{1}{a}(c-a-a^2)\right) + o(\mu_1), \tag{17}$$

which together with the heteroclinic orbit along the x_1 axis form a heteroclinic cycle. The invariant cycle born at the Neimark-Sacker bifurcation disappears when it simultaneously collides with the two saddles forming the heteroclinic cycle.

If $a < 0$, $b > 0$ and $\mu_1 < 0$ the saddles $Q_\pm$ do not exist. In this case the invariant cycle born at the Neimark-Sacker bifurcation grows, until it blows up and disappears from any fixed phase space domain at some curve B. This global bifurcation can not be analyzed in the local context of the normal forms, because the limit cycle always grows up to the boundary of the domain of validity of the normal form analysis (that is only valid in a neighborhood of the fixed point whose stability is analyzed). It is even possible that the invariant curve loses its smoothness and disappears before touching the boundary of the domain of validity of the normal form.

From the S symmetry ($x_2 \to -x_2$) that the ODE (13) inherits from the map, we see that the $x_2 = 0$ horizontal axis is an invariant curve, and the trajectories do not cross it. Therefore the half plane $x_2 > 0$ is invariant, and once the trajectories and phase portrait on the upper half plane $x_2 > 0$ have been found, the action of S gives the dynamics on the lower half plane $x_2 < 0$. The phase portraits of the ODE (13) restricted to the upper half plane are almost identical to the phase portraits of the fold-Hopf bifurcation [16,18]. A brief summary of the four different scenarios, depending on the signs of a and b follows. Scenario I is analyzed in more detail because it is the most complex of the four scenarios, and it is the one that takes place in the pipe flow problem that motivated this normal form analysis.

Figure 2 shows the bifurcation diagram of the ODE (13) corresponding to the scenario I, $a > 0$ and $b > 0$. There are four bifurcation curves. Two of them are common to all scenarios, the fold curve F where the fixed points $Q_\pm$ are born, and the pitchfork curve Pf where $P_\pm$ are born. There are also the Neimark-Sacker curve NS where an invariant cycle is born from $P_\pm$, and the Het curve where this invariant cycle collides simultaneously with $Q_\pm$ forming a heteroclinic cycle and disappears. The shaded areas in the phase portraits of Fig. 2 are invariant regions where all trajectories starting within them remain close to the origin forever, whereas those starting outside escape away from the domain of validity of the normal form analysis.

The orbit structure of the map close to the heteroclinic collision is generically different from the orbit structure of the

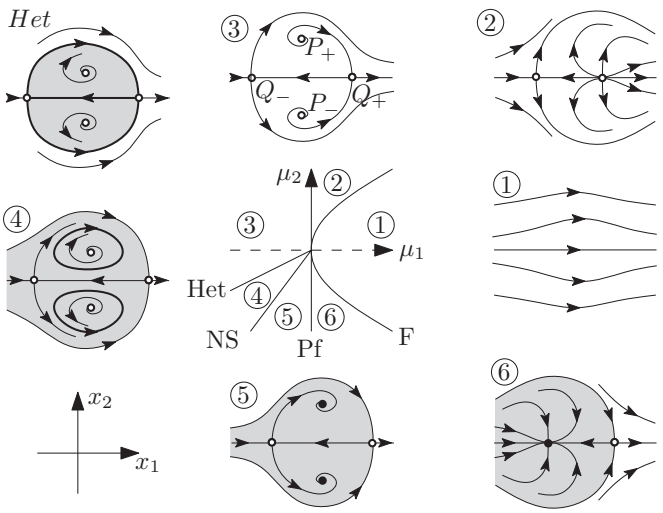

FIG. 2. Bifurcation diagram of the ODE (13) corresponding to scenario I: $a > 0$ and $b > 0$.

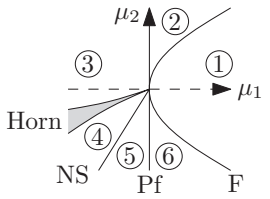

FIG. 3. Regime diagram of the map (7), corresponding to the scenario I of the approximating ODE (13) shown in Fig. 2; the horn of complexity and chaotic dynamics is shown in gray.

approximating ODE. The coincidence of the stable manifold of Q_+ and the unstable manifold of Q_- occurring for $\phi^1(x,\mu)$ is generically replaced by their transversal intersection, giving rise to a heteroclinic structure displaying chaotic dynamics [18]. The transversal heteroclinic structure exists in an exponentially narrow parameter region around the Het curve, bounded by two smooth bifurcation curves corresponding to homoclinic tangencies. This shadowed region (denoted by Horn) is depicted in gray in Fig. 3, that shows the regime diagram of the map (7), corresponding to the scenario I of the approximating ODE (13) shown in Fig. 2. The only difference is that the curve Het is replaced by the horn.

Figure 4 shows the formation of the heteroclinic cycle, and instead of schematics it shows numerically computed phase portraits of the map (7) for $a = 1.05$, $b = 0.5$, $c = -0.53$, and $d = -1.5$. We move inside the horn along a vertical path corresponding to $\mu_1 = -0.1$. In Fig. 5 we see the tangency between the stable manifold of Q_+ and the unstable manifold of Q_- when entering the horn in Fig. 5(a), the transversal intersection between them inside the horn in Fig. 5(b), and the tangency again on exiting the horn in Fig. 5(c). The dynamics inside the horn is of Silnikov type, with an infinity of unstable limit cycles and the presence of a chaotic attractor [18].

Figure 6 shows the bifurcation diagram corresponding to the scenario II, $a < 0$ and $b > 0$. In this scenario the Neimark-Sacker curve exists but the invariant circle does not coexist with the $Q_\pm$ fixed points, so the heteroclinic collision can not exist. In this scenario the invariant circle disappears because it grows until it collides with the boundary of the domain along a curve B. The real fate of the invariant circle depends on properties of the dynamical system outside of the domain of validity of the normal form analysis; it is even possible that the invariant circle looses its smoothness and disappears before touching the boundary of the domain [16].

In both scenarios I and II the relative position between the Neimark-Sacker curve NS and the curve where the invariant cycle is destroyed (Het in scenario I and B in scenario II) depends on the specific values of the constants a, b, c, and d. In particular it depends on the value of the first Liapunov coefficient of the Neimark-Sacker bifurcation, given by [16]

$$\ell_1 = \tfrac{1}{2}(-a^2 b - 3ab - ad + bc) + o(\mu_1). \qquad (18)$$

If $\ell_a < 0$ the bifurcation is supercritical and the invariant cycle is stable, and the complex dynamics inside the horn is observable, which is the case depicted in Figs. 2 and 6, and it is the case that happens in the pipe flow problem. If $\ell_a > 0$ the bifurcation is subcritical and the invariant cycle and chaotic

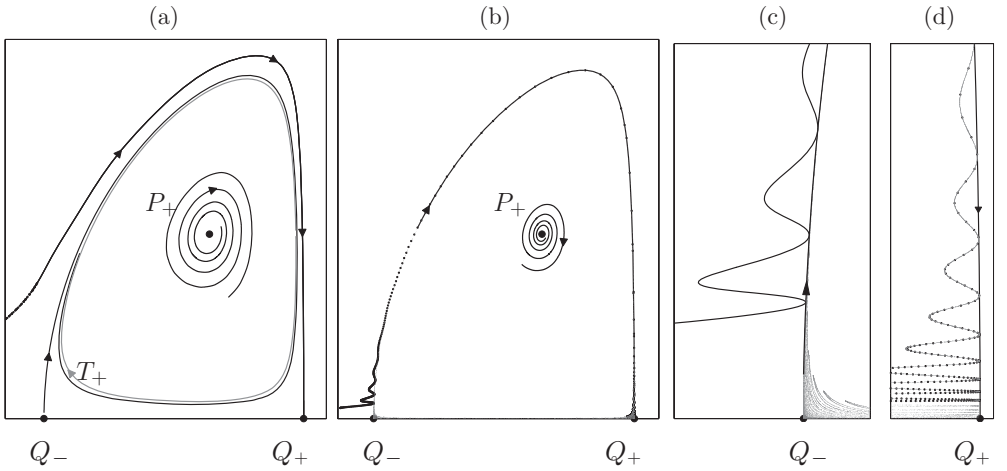

FIG. 4. Formation of the heteroclinic cycle. (a) the invariant curve born at the NS bifurcation is stable, but approaching both $Q_\pm$ at $\mu_2 = 0.15$. (b) The heteroclinic cycle has just appeared at $\mu_2 = 0.15925$. (c) and (d) are closeups near $Q_\pm$, showing the tangency between the stable manifold of Q_- and the unstable manifold of Q_+.

attractor are unstable. The additional nondegeneracy condition $\ell_1 \neq 0$ has been assumed in the analysis.

The remaining scenarios III and IV are much simpler, because the invariant circle does not exist, and we have only fixed points and the fold and pitchfork local bifurcation curves. Bifurcation diagrams for these two cases are depicted in Fig. 7.

The governing equations of the pipe flow are the Navier-Stokes equations, a system of PDEs. In this problem the map appears when studying the stability of periodic solutions (traveling waves) via a Poincaré map. Therefore, the fixed points of the map become limit cycles of the PDE, and the invariant cycle becomes a two-torus (a modulated traveling wave). The horn of complexity corresponds to the destruction of the two-torus and the formation of a chaotic attractor.

III. EXAMPLE IN PIPE-POISEUILLE FLOW

The analysis of the fold-pitchfork bifurcation presented here was initially motivated by the phenomena observed along a supercritical bifurcation cascade of nonlinear traveling waves in pipe-Poiseuille flow [14]. There was evidence that the eventual formation and later destruction of a chaotic set along the cascade resulted from a global bifurcation conditioned by the presence of symmetries.

Pipe flow is invariant under all azimuthal rotations about the axis and reflections with respect to all diametral planes, as well as under all axial translations $[\mathrm{O}(2)_\theta \times \mathrm{SO}(2)_z]$. The traveling wave (tw) at the origin of the sequence of transitions has broken all continuous symmetries, but preserves some discrete remnants of the $\mathrm{SO}(2)_\theta \times \mathrm{SO}(2)_z$: it is periodic in both the axial and azimuthal coordinates, with wave numbers $\kappa = 1.63$ and $n = 2$, respectively. Thus, it is invariant under discrete axial shifts of $\lambda = 2\pi/\kappa \simeq 3.85D/2$, where D is the pipe diameter, and under azimuthal rotations generated by the cyclic group C_2. The wave has an additional nontrivial discrete

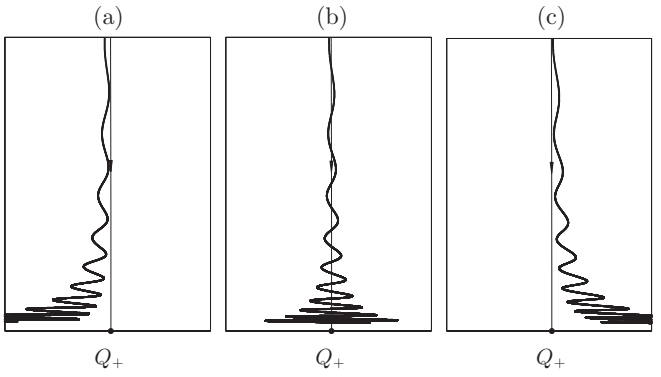

FIG. 5. Moving across the horn with the heteroclinic structure; views of the stable manifold of Q_- close to Q_+. (a) entering the horn at $\mu_2 = 0.159\,20$; (b) inside the horn at $\mu_2 = 0.159\,35$; (c) exiting the horn at $\mu_2 = 0.159\,50$.

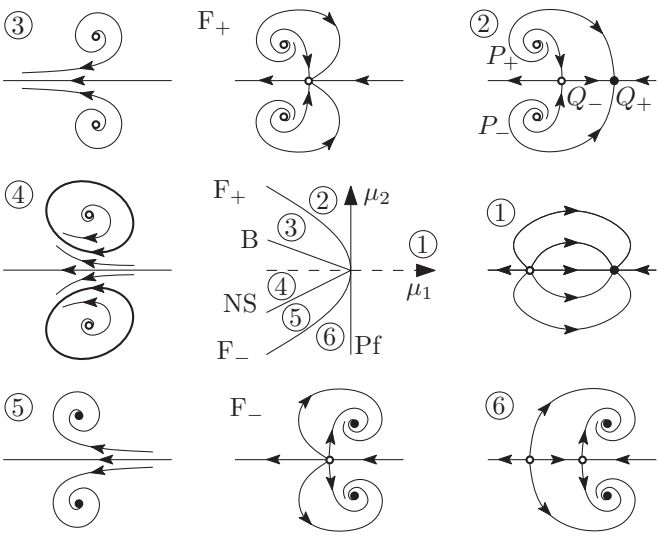

FIG. 6. Bifurcation diagram corresponding to scenario II: $a < 0$ and $b > 0$.

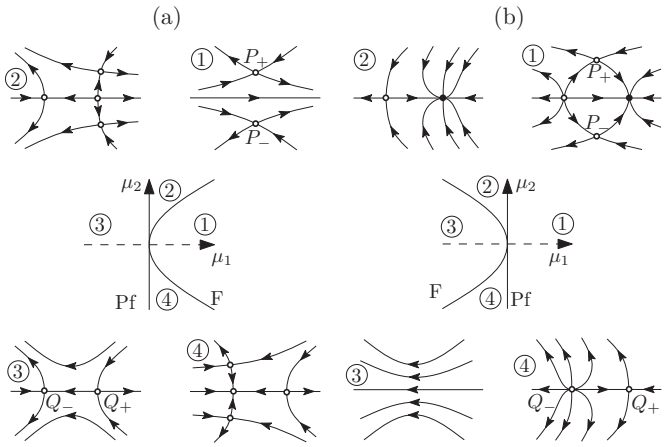

FIG. 7. Bifurcation diagram corresponding to scenarios (a) III: $a > 0$ and $b < 0$; and (b) IV: $a < 0$ and $b < 0$.

symmetry (shift-reflect)

$$Su(x) = S(u,v,w)(r,\theta_i + \theta, z; t) = (u,-v,w)(r,\theta_i - \theta, z + \pi/\kappa; t), \quad (19)$$

which leaves it unaltered when shifted half a wavelength downstream and then reflected with respect to any of two diametral planes tilted with $\theta_i = \theta_0$ and $\theta_i = \theta_0 + \pi/2$, where θ_0 parametrizes the azimuthal degeneracy of solutions. The S symmetry is a remnant version of the reflection symmetry with respect to all diametral planes that was part of the $O(2) = SO(2) \rtimes Z_2$ azimuthal symmetry group. S plays the role of the symmetry that modifies the 1:1 strong resonance scenario into the fold-pitchfork studied here. This symmetry becomes apparent by plotting the traveling wave z-averaged axial velocity contours of Fig. 8(a), which also show the streaky structure of the wave, consisting of two high-speed streaks, each sandwiched between a couple of low-speed streaks. The streaks are in stationary equilibrium with two pairs of counterrotating vortices as evidenced by the couple of axial vorticity isosurfaces on the right.

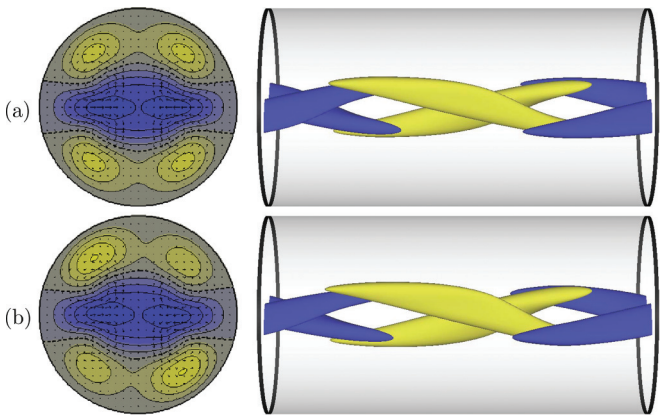

FIG. 8. (Color online) Traveling waves at $(\mathrm{Re},\kappa) = (2215, 1.63)$, from Ref. [14]. Left: z-averaged cross-sectional axial velocity contours spaced at intervals of $\Delta\langle u_z\rangle_z = 0.1\,U$. In-plane velocity vectors are also displayed. Right: axial vorticity isosurfaces at $\omega_z = \pm U/D$. Fluid flows rightwards. Blue (dark gray) for negative, Yellow (light) for positive. (a) traveling wave (tw), (b) spiraling wave (sw_+).

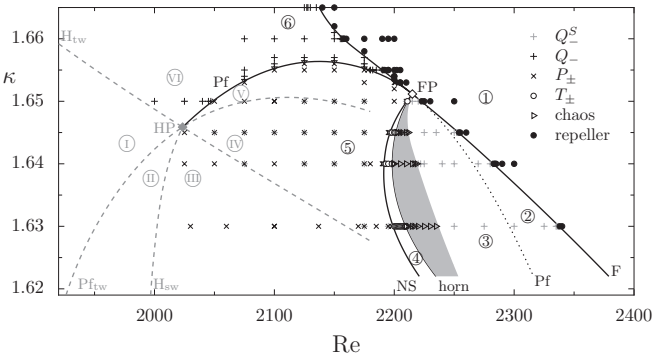

FIG. 9. Bifurcation diagram in (Re,κ)-parameter space corresponding to the pipe-Poiseuille problem. Black solid lines represent numerically identified discrete-time bifurcation curves: fold (F), pitchfork (Pf), and Neimark-Sacker (NS). They delimit the region of existence of the different types of solutions (marked with symbols as explained in the legend). The black dotted line illustrates the inaccessible part of Pf. The shaded region is the horn where chaotic dynamics occur. Bifurcation of relative equilibria are indicated by dashed lines. The two diamond symbols correspond to the two codimension-two points: gray filled diamond for the Hopf-pitchfork of relative equilibria (HP), open diamond for the fold.-pitchfork of maps (FP). The circled numbers identify regions of Fig. 2 (arabic, corresponding to scenario I of Fig. 1) and Fig. 10(a) (roman).

The bifurcation cascade was unfolded in Ref. [14] by varying a single parameter: the Reynolds number, defined as $\mathrm{Re} = UD/\nu$, where U is the mean axial speed of the flow and ν the kinematic viscosity of the fluid. Their main results correspond to the straight path at $\kappa = 1.63$ in Fig. 9. For a detailed description of the numerical methods employed to compute the solutions and track the bifurcation curves see Ref. [15]. As a result of increasing Re at fixed κ, tw undergoes a supercritical pitchfork bifurcation ($\mathrm{Pf_{tw}}$) that breaks the shift-reflect symmetry and two symmetry-conjugate branches of spiraling waves ($\mathrm{sw}_\pm$, simultaneously traveling and rotating) are issued. The flow structure of the spiraling waves is extremely close to that of the traveling wave, but the shift-reflect symmetry has been disrupted, as is evident from Fig. 8(b). All these waves are relative equilibria, so that the dynamics along the drift direction is trivial and decouples from the dynamics orthogonal to the drift [21]. Monitoring drift-independent quantities provides a straightforward method of analyzing bifurcations of drifting solutions. At slightly higher Re, both waves become unstable in supercritical Hopf bifurcations and two branches of modulated waves, one traveling and the other spiraling, emerge. These waves are relative periodic orbits and become discrete-time equilibria when a Poincaré section Π based on some drift-independent quantity is defined and the associated Poincaré map Π is considered, as illustrated in Fig. 10(b). The modulated traveling waves (gray plus signs, Q_-, appearing to the right of $\mathrm{H_{tw}}$), which are unstable at onset, can be followed to higher Re by restricting the computations to the symmetry space they inhabit. It is found that the branch extends all the way up to a point where it bends back in a fold of relative cycles (F) producing a branch of saddle orbits (Q_+) that can be computed but at a high computational cost, which makes branch continuation unfeasible with bare time evolution. Beyond the fold, no solution remains in this

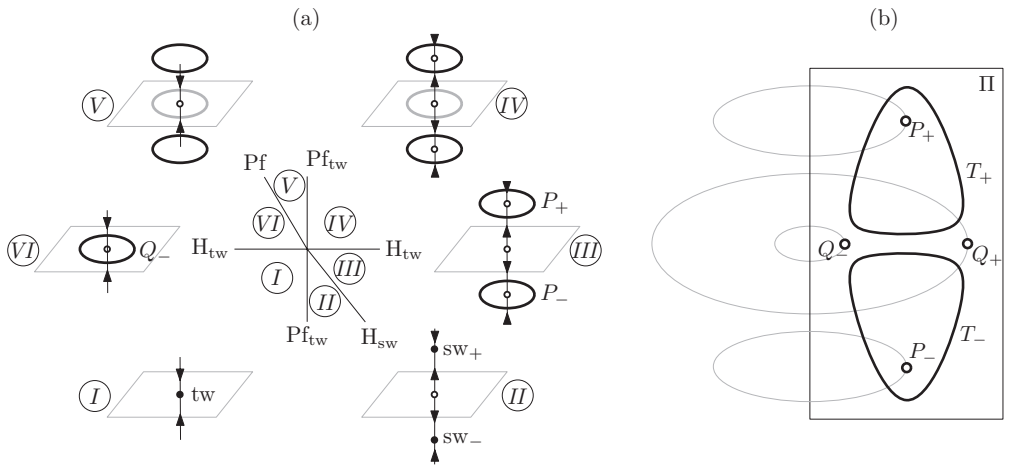

FIG. 10. (a) Bifurcation diagram of the Hopf-Pitchfork bifurcation, for the scenario corresponding to the present pipe problem. Solid fixed points are stable, hollow ones unstable; black/gray limit cycles are stable/unstable. The gray plane is the Z_2-symmetric subspace. (b) Poincaré section Π of the limit cycle solutions ($P_\pm$ and Q_-) in (a), including other solutions not associated with the Hopf-Pitchfork scenario: Q_+, born alongwith Q_- in a remote fold (F curve in Fig. 9), and the two-tori $T_\pm$, born in the Neimark-Sacker bifurcation curve NS. The phase portrait shown in (b) corresponds to region ④ in Fig. 9.

region of phase space and the flow is left free to evolve elsewhere (black circles). Meanwhile, the modulated spiraling waves (crosses, $P_\pm$, appearing to the right of H_{sw}) undergo a supercritical Neimark-Sacker bifurcation (NS) and a branch of doubly modulated spiraling waves, discrete-time cycles when the purposely defined comoving Poincaré map is considered, is created (open circles, $T_\pm$). These waves can be seen as relative tori, so that drift-independent quantities revolve on an invariant two-torus. The doubly modulated spiraling waves grow large in a short range of Re and suddenly incorporate mild temporal chaos (triangles within the shaded horn). For higher Re, the chaotic attractor thus formed opens up and no stable structure capable of sustaining permanent dynamics remains in this region of phase space.

To analyze the bifurcation scenario in detail, we have undertaken a comprehensive exploration of the two-dimensional parameter space (Re,κ), illustrated in Fig. 9 using the numerical solvers in [14]. Continuation of the Pf_{tw}, H_{tw} and H_{sw} bifurcation curves shows that they intersect in a codimension-2 Hopf-pitchfork point (HP). This bifurcation has been extensively studied in Refs. [22] and [23], and the various scenarios that arise closely resemble those of the double Hopf bifurcation discussed in Ref. [18] (case IV, where the amplitude dynamics induced by one of the two pairs of imaginary eigenvalues must be interpreted here as the dynamics away from the Z_2-symmetric subspace). Figure 10(a) schematically depicts the bifurcation diagram corresponding to the particular scenario of the problem at hand. The tw of region ① generates sw in region ②, which in turn give rise to modulated spiraling waves $P_\pm$ in region ③. Again tw generates a modulated traveling wave Q_- in region ④, adding the last ingredients that are needed for the Fold-Pitchfork bifurcation to take place. It is precisely by defining a Poincaré section Π with some drift-independent quantity, intersecting transversally all modulated waves, which the continuous-time system reduces to a discrete-time dynamical system or map. In this description, traveling and spiraling waves have no longer a representation, modulated waves become fixed points, and doubly modulated waves are nothing but discrete-time cycles. The relation between the original continuous-time system and the discrete-time system is illustrated in Fig. 10(b), taken to the far right of region ⑤, beyond the Neimark-Sacker bifurcation. By applying the Poincaré section, the modulated traveling wave is reduced to a fixed point of the map (Q_-), and also the modulated spiraling waves ($P_\pm$), while the doubly modulated spiraling waves, which are relative tori, result in discrete-time cycles ($T_\pm$). Moving to region ⑤ $sw_\pm$ disappear in Pf_{tw}. Finally, the modulated spiraling waves ($P_\pm$) also disappear in region ⑥ $sw_\pm$ after colliding with the modulated traveling wave Q_- (black plus signs), which regains stability in a pitchfork of cycles Pf. This is the only bifurcation curve that keeps a representation in the discrete-time system resulting from the Poincaré section. In fact, it is the very same pitchfork of equilibria Pf that is central to the fold-pitchfork bifurcation of maps under study.

The $\kappa = 1.63$ path described above is reminiscent of case I of Fig. 1 and would correspond to a one-dimensional path crossing all regions but ⑥ in Fig. 2. Instead, the pitchfork relating Q_- and $P_\pm$, due to the presence of HP, happens to be mediated by intervening relative equilibria. As already discussed, in this parameter region Q_- and $P_\pm$ result from Hopf bifurcations of relative equilibria that are in turn related by a pitchfork. The occurrence of HP, from which Pf is issued, is therefore crucial in the sense that it sets the stage for the complete unfolding of the fold-pitchfork bifurcation of the Poincaré map associated to comoving stroboscopic freezing of the waves' traveling and modulational character. In fact, regions ④ and ⑤ are indistinguishable in the discrete-time setting and merge together into region ⑤ of the fold pitchfork bifurcation for maps, while region ⑥ has direct correspondence with region ⑥.

A thorough exploration of parameter space helps identify the codimension-two point (FP) where F, Pf, NS, and the chaotic "horn" meet. All the curves depicted are accessible through time-stepping, exception made of the dotted branch of Pf. The fold-pitchfork bifurcation predicts that the branch

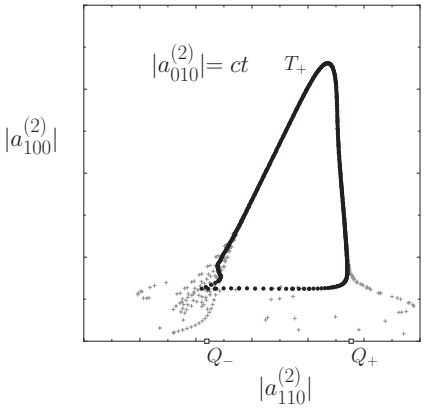

FIG. 11. Poincaré section for $\kappa = 1.63$, Re $= 2209.6725$ (T_+, black circles) and Re $= 2209.6726$ (chaotic solution, gray plus signs). The section is defined by $|a^{(2)}_{010}| =$ ct and shows $|a^{(2)}_{100}|$, which vanishes for shift-reflect solutions, against $|a^{(2)}_{110}|$. $Q_\pm$ are represented with open squares on the x axis.

of $P_\pm$, which is pitchfork-related at one end with Q_-, must fuse with Q_+ in another supercritical pitchfork at the other end. Neither Q_+ nor $P_\pm$ are accessible through time stepping in this parameter region, so identification of Pf would require more sophisticated numerical techniques [24,25].

Analysis of the normal form for the fold-pitchfork bifurcation detected that manifold tangencies precluded the formation of a neat heteroclinic cycle. Figure 11 tests this hypothesis by approaching the horn of chaotic dynamics from region ④. It corresponds to increasing Re at $\kappa = 1.63$, and using the moduli of three expansion coefficients to represent drift-independent phase map trajectories. A streamwise-independent coefficient ($|a^{(2)}_{010}|$) is used to define the comoving Poincaré section, a mixed coefficient ($|a^{(2)}_{110}|$) is taken to represent x_1, and an appropriately chosen axisymmetric coefficient ($|a^{(2)}_{100}|$) that vanishes exactly for shift-reflect symmetric solutions, plays the role of x_2. At Re $= 2209.6725$ the cycle T_+ (black dots) has grown large around P_+ (now unstable), while adopting a triangle shape whose bottom side is aligned with the shift-reflect symmetric subspace. The right lower vertex of the cycle is approaching Q_+, while the left vertex seems to be conforming to the folds of the stable manifold of Q_+ as Q_- is approached. At a slightly higher Re $= 2209.6726$, the stable manifold of Q_+ has gone beyond tangency with the unstable manifold of Q_-, and the attractor within the horn incorporates time-chaotic dynamics, as is clear from the cloud of gray plus signs in the vicinity of Q_- in Fig. 11. The chaotic dynamics persist within the horn and become transient, with ulterior bursts and eventual decay to laminarity, when crossing to region ③. This crossing is relatively clear for $\kappa \geqslant 1.64$, but not at $\kappa = 1.63$, where the transition seems to be complicated by factors that are extrinsic to the fold-pitchfork bifurcation framework.

IV. CONCLUSION

We have performed a combined analysis of the dynamics of modulated traveling waves in pipe flow, using extensive direct numerical simulations of the Navier-Stokes equations, combined with dynamical systems theory and normal form analysis. The main result is that the interplay of the modulated traveling waves resulting in chaotic dynamics is governed by a couple of codimension-two bifurcations that act as organizing centers of the dynamics. One of them is a Hopf-pitchfork bifurcation HP, which could already be surmised from Ref. [14], and whose detailed mathematical analysis is not novel. In this bifurcation, from the original Z_2-symmetric traveling wave solution tw, several drifting (traveling and/or spiraling) modulated wave (MW) solutions emerge. The interaction among these MW and the corresponding heteroclinic dynamics and transition to chaos is governed by the second codimension-two bifurcation, a fold-pitchfork bifurcation for maps FP. The maps are obtained via a convenient Poincaré section of the MW in the comoving frame, getting rid of the two frequencies in the process, so that MW become fixed points of the map. The codimension-two FP bifurcation had not been studied previously. It is a specific Z_2 version of the 1:1 strong resonance bifurcation. The presence of the flip-reflect symmetry greatly modifies the dynamics, that bears strong similitude with the fold-flip bifurcation of maps recently analyzed in Ref. [16]. We have presented a detailed analysis of this bifurcation closely following the fold-flip study, presenting bifurcation diagrams for the four different possible scenarios, and analyzing in detail the most complex case, which includes heteroclinic dynamics and a horn of chaotic dynamics. This complex case is the scenario observed for the pipe flow waves under consideration. The analysis of the waves involved and their bifurcations leading to a chaotic set are a relevant step to the understanding of subcritical transition and turbulence sustainment in shear flows.

We present a discrete-time (using a Poincaré section) codimension-two bifurcation within the framework of pipe flow nonlinear stability analysis. Previous studies had mainly addressed the computation and Reynolds number continuation of Navier-Stokes relative equilibria and periodic orbits, but the pipe length (or, equivalently, the fundamental streamwise wave number κ) has rarely been considered as a bifurcation parameter [15]. Streamwise length of shear parallel flows has long been known to be a key element in turbulence sustainment and decay [26]. In particular, the generic transition scenario in pipe flow is characterized by the phenomenon of intermittency or streamwise localization of turbulence, where a competition between two antagonistic tendencies, one to decay the other to spread, occurs [27]. Many unstable solutions in the form of traveling and modulated traveling waves have been found in recent years [7,13] that are believed to partake in the chaotic set governing subcritical transition to turbulence [28]. This transition exhibits slow dynamics, like the decay and/or splitting of puffs, that are reminiscent of homoclinic or heteroclinic dynamics. Our analysis unravels precisely a source of such kind of slow dynamics. The bifurcation scenario studied here takes place at Reynolds numbers for which the first pipe flow localized instabilities typically occur. Although the connection between the codimension-two bifurcation studied in this work and turbulence sustainment requires further analysis, we believe it will certainly rely on the detailed knowledge of fundamental heteroclinic phase space dynamics such as those analyzed here.

APPENDIX A: HYPERNORMAL FORM

We want to transform the normal form (5) into

$$y_1 \to \tilde{f}_1(y,\alpha) = \sigma_1 + \sigma_2 y_1 + \tfrac{1}{2}G_{20}y_1^2 + \tfrac{1}{2}G_{02}y_2^2 + \tfrac{1}{6}G_{30}y_1^3 + \tfrac{1}{2}G_{12}y_1y_2^2, \quad \text{(A1a)}$$

$$y_2 \to \tilde{f}_2(y,\alpha) = y_2 + H_{11}y_1y_2, \quad \text{(A1b)}$$

by means of the transformation (6). By using (5), (6), and (A1) in the identity $\tilde{f}(\Lambda(x)) = \Lambda(f(x))$, we obtain a system of ten equations for the ten coefficients of Λ and $\tilde{f}$, as functions of the coefficients of f. In detail,

$$\tilde{f}_1(\Lambda(x)) = \sigma_1 + \sigma_2\Lambda_1 + \tfrac{1}{2}G_{20}\Lambda_1^2 + \tfrac{1}{2}G_{02}\Lambda_2^2 + \tfrac{1}{6}G_{30}\Lambda_1^3 + \tfrac{1}{2}G_{12}\Lambda_1\Lambda_2^2, \quad \text{(A2a)}$$

$$\tilde{f}_2(\Lambda(x)) = \Lambda_2 + H_{11}\Lambda_1\Lambda_2, \quad \text{(A2b)}$$

$$\Lambda_1(f(x)) = \epsilon + f_1 + \tfrac{1}{2}Af_1^2 + \tfrac{1}{2}Bf_2^2 \quad \text{(A2c)}$$

$$\Lambda_2(f(x)) = f_2, \quad \text{(A2d)}$$

and identifying equal powers of x_1 and x_2 up to third order included, we arrive at

$$\sigma_1 + \epsilon\sigma_2 + \epsilon^2G_{20}/2 + \epsilon^3G_{30}/6 = \epsilon + \sigma + A\sigma^2/2 \quad \text{(A3a)}$$

$$B\sigma_2 + \epsilon BG_{20} + G_{02} + \epsilon^2BG_{30}/2 + \epsilon G_{12} = (1+A\sigma)g_{02} + \lambda_2^2B \quad \text{(A3b)}$$

$$\sigma_2 + \epsilon G_{20} + \epsilon^2G_{30}/2 = (1+\sigma A)\lambda_1 \quad \text{(A3c)}$$

$$BG_{20} + \epsilon BG_{30} + G_{12} = (1+\sigma A)g_{12} + \lambda_1Ag_{02} + 2\lambda_2Bh_{11} \quad \text{(A3d)}$$

$$A\sigma_2 + (1+\epsilon A)G_{20} + \epsilon(1+\epsilon A/2)G_{30} = \lambda_1^2A + (1+\sigma A)g_{20} \quad \text{(A3e)}$$

$$AG_{20} + (1+3\epsilon A)G_{30}/3 = \lambda_1Ag_{20} + (1+\sigma A)g_{30}/3 \quad \text{(A3f)}$$

$$1 + \epsilon H_{11} = \lambda_2 \quad \text{(A3g)}$$

$$BH_{11} = h_{03}/3 \quad \text{(A3h)}$$

$$H_{11} = h_{11} \quad \text{(A3i)}$$

$$AH_{11} = h_{21} \quad \text{(A3j)}$$

The last four equations give

$$\epsilon = \frac{\lambda_2 - 1}{h_{11}}, \quad A = \frac{h_{21}}{h_{11}}, \quad B = \frac{h_{03}}{3h_{11}}, \quad H_{11} = h_{11}, \quad \text{(A4)}$$

where we have used the fact that $h_{11}(0) \neq 0$, and therefore $h_{11}(\alpha) \neq 0$ for small enough α values. The remaining six equations are linear in the coefficients of $\tilde{f}_1$, and the determinant value is $1/3$, so the solution exists and is unique. Explicit expressions are

$$\begin{aligned}
\sigma_1 &= \epsilon + \sigma - [1+\epsilon A(1+\epsilon A)/2](1+\sigma A)\epsilon\lambda_1 + (1+\epsilon A)\epsilon^2A\lambda_1^2 + \sigma^2A/2 + [(1+\sigma A)(1+\epsilon A) - \epsilon A\lambda_1]\epsilon^2g_{20}/2 \\
&\quad - (1+\sigma A)\epsilon^3g_{30}/6, \\
\sigma_2 &= (1+\epsilon A + 3\epsilon^2A^2/2)(1+\sigma A)\lambda_1 + \left[3\epsilon A\lambda_1/2 - (1+3\epsilon A/2)(1+\sigma A) - (1+3\epsilon A/2)\epsilon A\lambda_1^2\right]\epsilon g_{20} \\
&\quad + (1+\sigma A)\epsilon^2g_{30}/2, \\
G_{20} &= (1+3\epsilon A)A\lambda_1^2 - (1+3\epsilon A)(1+\sigma A)A\lambda_1 + [(1+3\epsilon A)(1+\sigma A) - 3\epsilon A\lambda_1]g_{20} - (1+\sigma A)\epsilon g_{30}, \quad \text{(A5)}
\end{aligned}$$

$$\begin{aligned}
G_{02} &= B\lambda_2^2 - (1+\epsilon A)(1+\sigma A)B\lambda_1 + B\epsilon A\lambda_1^2 + (1+\sigma A)\epsilon Bg_{20} + (1+\sigma A - \epsilon A\lambda_1)g_{02} - (1+\epsilon A)\epsilon g_{12} - 2\epsilon B\lambda_2h_{11}, \\
G_{30} &= 3(1+\sigma A)A^2\lambda_1 - 3A^2\lambda_1^2 + (1+\sigma A)g_{30} + 3(\lambda_1 - 1 - \sigma A)g_{20}, \quad \text{(A6)} \\
G_{12} &= (1+\sigma A - \lambda_1)AB\lambda_1 + A\lambda_1g_{02} + 2B\lambda_2h_{11} + (1+\sigma A)(g_{12} - Bg_{20}).
\end{aligned}$$

Some additional transformations can be made in the normal form (A1). First, by scaling y_1, we can force $H_{11} = h_{11} = -1$ (the option $+1$ is also possible, but with -1 the results are closer to the normal forms in Ref. [16]). We can also introduce two new parameters, $\mu_1 = \sigma_1(\alpha)$ and $\mu_2 = \sigma_2(\alpha) - 1$, assuming the change of parameters is invertible. With all these transformations we arrive at (7).

APPENDIX B: FIXED POINTS AND THEIR LOCAL BIFURCATIONS

The fixed points of the map are obtained by solving $F(x,\mu) = x$

$$\begin{aligned}
\mu_1 + \mu_2x_1 + \tfrac{1}{2}ax_1^2 + \tfrac{1}{2}bx_2^2 + \tfrac{1}{6}cx_1^3 + \tfrac{1}{2}dx_1x_2^2 &= 0, \\
x_1x_2 &= 0.
\end{aligned} \quad \text{(B1)}$$

The second equation admits two solutions, $x_1 = 0$ and $x_2 = 0$. Let us start with $x_2 = 0$; we obtain the cubic equation

$$\mu_1 + \mu_2 x_1 + \tfrac{1}{2}a x_1^2 + \tfrac{1}{6}c x_1^3 = 0. \tag{B2}$$

For $\mu = 0$, the roots are a double zero and $x_1 = -3a/c$. If $a \neq 0$, the last root is away from the origin, and due to the continuity of the roots with parameters, will remain away from the origin for μ small. Therefore, in a local analysis, only the two roots close to the origin must be considered, and we assume from now on the nondegeneracy condition $a \neq 0$. These two roots coincide for $\mu = 0$, and in fact coincide along a curve of fold bifurcations. This curve can be computed as the loci of the points in parameter space where the polynomial (B2) has a double root

$$\begin{aligned} \mu_1 + \mu_2 x_1 + \tfrac{1}{2}a x_1^2 + \tfrac{1}{6}c x_1^3 &= 0, \\ \mu_2 + a x_1 + \tfrac{1}{2}c x_1^2 &= 0. \end{aligned} \tag{B3}$$

By eliminating x_1 we obtain the fold curve

$$x_1 = \frac{3c\mu_1 - a\mu_2}{a^2 - 2c\mu_2}, \tag{B4}$$

$$2a\mu_1 - \mu_2^2 = \frac{3c}{a^2}\left(2a\mu_1\mu_2 - c\mu_1^2 - \frac{8}{9}\mu_2^3\right). \tag{B5}$$

By expanding μ_1 and x_1 in powers of μ_2 we obtain at the SN curve

$$2a\mu_{1,\mathrm{SN}} = \mu_2^2\left(1 + \frac{1}{3}\frac{c\mu_2}{a^2} + \frac{7}{4}\left(\frac{c\mu_2}{a^2}\right)^2 + \cdots\right), \tag{B6}$$

$$x_{1,\mathrm{SN}} = -\frac{\mu_2}{a}\left(1 + \frac{1}{2}\frac{c\mu_2}{a^2} + \frac{1}{2}\left(\frac{c\mu_2}{a^2}\right)^2 + \cdots\right). \tag{B7}$$

We can now compute the two solutions emerging from the fold, by introducing $\mu_1 = \mu_{1,\mathrm{SN}} - \beta$ and $x_1 = x_{1,\mathrm{SN}} + \delta$ in (B2). As $\mu_{1,\mathrm{SN}}$ and $x_{1,\mathrm{SN}}$ satisfy (B3) we obtain

$$\beta = \tfrac{1}{2}a\delta^2 + \tfrac{1}{2}c x_{1,\mathrm{SN}}\delta^2 + \tfrac{1}{6}c\delta^3. \tag{B8}$$

In order to have solutions, $\mathrm{sign}(\beta) = \mathrm{sign}(a)$, so the two SN points exist to the left of the curve $2a\mu_1 = \mu_2^2 + O(\mu_2^3)$ if $a > 0$, and to the right if $a < 0$. By introducing $\beta = \frac{1}{2}a\epsilon^2$, where ϵ is a measure of the distance to the SN curve, we obtain

$$Q_\pm = \left(-\frac{\mu_2}{a} \pm \epsilon - \frac{c\mu_2^2}{2a^3} \pm \frac{c\mu_2\epsilon}{2a^2} - \frac{c\epsilon^2}{6a} + \mathrm{hot}, 0\right), \tag{B9}$$

$$\begin{aligned} \epsilon &= \frac{1}{a}\sqrt{2a\mu_{1,\mathrm{SN}} - 2a\mu_1} \\ &= \frac{1}{a}\sqrt{\mu_2^2 - 2a\mu_1 + \frac{c\mu_2^3}{3a^2} + O\left(\mu_2^4\right)}, \end{aligned} \tag{B10}$$

where hot stands for higher-order terms in μ_2 and ϵ. At lowest order,

$$Q_\pm = \left(\frac{1}{a}\left(-\mu_2 \pm \sqrt{\mu_2^2 - 2a\mu_1}\right) + \mathrm{hot}, 0\right). \tag{B11}$$

The stability of these fixed points is determined by the eigenvalues of the Jacobian of the map F at the fixed points,

$$D_x F = \begin{pmatrix} 1 + \mu_2 + a x_1 + \frac{1}{2}c x_1^2 + \frac{1}{2}d x_2^2 & b x_2 + d x_1 x_2 \\ -x_2 & 1 - x_1 \end{pmatrix}.$$

At $Q_\pm$,

$$D_x F(Q_\pm) = \begin{pmatrix} 1 + \mu_2 + a x_1 + \frac{1}{2}c x_1^2 & 0 \\ 0 & 1 - x_1 \end{pmatrix}, \tag{B12}$$

and the eigenvalues are

$$\begin{aligned} &\lambda_1(Q_\pm) = 1 + \mu_2 + a x_1 + \tfrac{1}{2}c x_1^2 = 1 \pm \sqrt{\mu_2^2 - 2a\mu_1} + \mathrm{hot} \\ &\lambda_2(Q_\pm) = 1 - x_1, \quad \mathrm{sign}\, x_1(Q_\pm) = -\,\mathrm{sign}(a\mu_2). \end{aligned}$$

Both eigenvalues are real. Eigenvalues with modulus larger (smaller) that one correspond to unstable (stable) directions. Therefore, the nature of the $Q_\pm$ points depends on $\mathrm{sign}(a\mu_2)$ (for ϵ small enough, i.e., close to the SN curve). If $a\mu_2 < 0$, one of the Q points is a saddle (one stable direction and the other unstable) and the other point is stable; if $a\mu_2 > 0$, one point is a saddle and the other point is a repeller (both directions unstable).

Let us now consider the fixed points with $x_1 = 0$. In this case we obtain two additional fixed points,

$$P_\pm = (0, \pm\sqrt{-2\mu_1/b}), \tag{B13}$$

that exist only if $b\mu_1 < 0$, i.e., at one side of the straight line $\mu_1 = 0$: to the left if $b > 0$, and to the right if $b < 0$. We will assume from now on the additional nondegeneracy condition $b \neq 0$. The two new fixed points are symmetrically related: $SP_+ = P_-$. On the line $\mu_1 = 0$ both fixed points $P_\pm$ merge and disappear, and moreover they coincide with one of the $Q_\pm$: $P_+ = P_- = (0,0) = Q_+$ for $\mu_2 > 0$, and Q_- for $\mu_2 < 0$. Therefore, on the line $\mu_1 = 0$ a pitchfork bifurcation of one of the symmetric states $Q_\pm$ takes place, and a couple of symmetrically related fixed points are born. For this reason we have named this bifurcation a fold-pitchfork bifurcation of maps. At $\mu_1 = \mu_2 = 0$ the four points merge at the origin.

We can compute the eigenvalues at the fixed points $P_\pm$ as before

$$\begin{aligned} D_x F(P_\pm) &= \begin{pmatrix} 1 + \mu_2 + \frac{1}{2}d x_2^2 & b x_2 \\ -x_2 & 1 \end{pmatrix} \\ &= \begin{pmatrix} 1 + \mu_2 - d\mu_1/b & \pm b\sqrt{-\frac{2\mu_1}{b}} \\ \mp\sqrt{-\frac{2\mu_1}{b}} & 1 \end{pmatrix}. \end{aligned} \tag{B14}$$

The eigenvalues of $P_\pm$ are the same, both points have the same stability properties. The eigenvalues are

$$\begin{aligned} \lambda_j(P_\pm) = 1 &+ \frac{1}{2}\left(\mu_2 - \frac{d}{b}\mu_1\right) \\ &+ \frac{(-1)^j}{2}\sqrt{\left(\mu_2 - \frac{d}{b}\mu_1\right)^2 + 8\mu_1}. \end{aligned}$$

If $\mu_1 > 0$, $P_\pm$ is a saddle; if $-(\mu_2 - d\mu_1/b)^2/8 < \mu_1 < 0$ the two eigenvalues are real and the two points $P_\pm$ are stable (unstable) if $\mu_2 - d\mu_1/b < 0$ (> 0). The only change of stability so far, at $\mu_1 = 0$, corresponds to the pitchfork bifurcation.

For $\mu_1 \leqslant -(\mu_2 - d\mu_1/b)^2/8 \leqslant 0$ the two eigenvalues are complex, with modulus $|\lambda_j|^2 = 1 + \mu_2 - (d/b + 2)\mu_1$. Therefore a Neimark-Sacker bifurcation of both $P_\pm$ takes place on the curve $\mu_2 = (d/b + 2)\mu_1$, $\mu_1 \leqslant 0$; in this bifurcation an invariant curve is born around each of the fixed points $P_\pm$.

These points exist only if $b\mu_1 < 0$, therefore the Neimark-Sacker bifurcation only takes place if $b > 0$.

APPENDIX C: ODE APPROXIMATING THE MAP

Given a map

$$x \to F(x,\mu) = Lx + N(x,\mu), \tag{C1}$$

where L is a constant matrix and $N(x,\mu)$ are nonlinear terms (at least order two in x, but it can contain linear terms in the parameters μ), we want to obtain an ODE

$$\dot{x} = G(x,\mu) = \Lambda x + Y(x,\mu), \tag{C2}$$

such that the flow at $t = 1$ coincides with F up to a given order in (x,μ): $\phi^1(x,\mu) = F(x,\mu) + O(k)$. The flow $\phi^t(x,\mu)$ satisfies the equation (12) and the initial condition $\phi^0(x,\mu) = x$. In order to compute $\phi^t(x,\mu)$ as a power series in (x,μ), a method based on Picard iterations will be used.

Proposition 1. The flow of (12) $\phi^t(x,\mu)$ satisfies the integral equation

$$\phi^t(x,\mu) = e^{t\Lambda}x + \int_0^t e^{(t-\tau)\Lambda} Y(\phi^\tau(x,\mu),\mu)d\tau \tag{C3}$$

Proof. Let us write

$$\phi^t(x,\mu) = e^{t\Lambda}(x + \psi^t(x,\mu)). \tag{C4}$$

From $\phi^0(x,\mu) = x$ we obtain $\psi^0(x,\mu) = 0$. As $\phi^t(x,\mu)$ satisfies (12),

$$\partial_t\phi^t(x,\mu) = \Lambda\phi^t + e^{t\Lambda}\partial_t\psi^t(x,\mu) = \Lambda\phi^t + Y(\phi^t(x,\mu),\mu), \tag{C5}$$

and $\psi^t(x,\mu)$ satisfies

$$\partial_t\psi^t(x,\mu) = e^{-t\Lambda}Y(\phi^t(x,\mu),\mu). \tag{C6}$$

Integrating (C6) and using $\psi^0(x,\mu) = 0$,

$$\psi^t(x,\mu) = \int_0^t e^{-\tau\Lambda}Y(\phi^\tau(x,\mu),\mu)d\tau. \tag{C7}$$

By substituting ψ^t back into (C4) we obtain the desired result. ∎

As Y is nonlinear, the terms in ϕ^t of order k, ϕ^t_k, are given by (C3) in terms of lower-order terms. We must simultaneously solve (C3) and $\phi^1(x,\mu) = F(x,\mu)$ order by order in powers of x and μ. As some of the fixed points (10) have coordinates proportional to the square root of μ, we will consider from now on that the parameters μ are $O(x^2)$. Therefore a term of the form $x^p\mu^q$ is of order $p + 2q$. This justifies the inclusion of the linear terms in μ that appear in (7) into the nonlinear term N in (11).

At order one, $\phi^t_1(x,\mu) = e^{t\Lambda}x$ and $\phi^1_1 = e^\Lambda x = F_1 = Lx$. We arrive at the equation

$$e^\Lambda = L. \tag{C8}$$

This equation does not have a solution in general; for example if L is real with some negative eigenvalues, then it do not exists a real Λ satisfying it. One must resort in these cases to more convoluted strategies, like looking for iterates of F (see Ref. [18], Chap. 9), or replacing F by MF, with an appropriate constant matrix [16]. In the present problem, as L is the identity matrix, (C8) is easy to solve: $\Lambda = 0$. Then (C3) reduces to

$$\phi^t(x,\mu) = x + \int_0^t Y(\phi^\tau(x,\mu),\mu)d\tau. \tag{C9}$$

The iterative procedure to solve this equation is given by the following.

Proposition 2. The nonlinear terms in $Y(x,\mu)$ and $\phi^t(x,\mu)$ can be computed iteratively for $k \geqslant 2$ as:

$$H_k(x,\mu,t) = \int_0^t \left(Y_{(k-1)}\left(\phi^\tau_{(k-1)}(x,\mu),\mu\right)\right)_k d\tau, \tag{C10}$$

$$Y_k(x,\mu) = N_k(x,\mu) - H_k(x,\mu,1), \tag{C11}$$

$$\phi^t_k(x,\mu) = tY_k(x,\mu) + H_k(x,\mu,t). \tag{C12}$$

where the subindex (m) indicates all the terms up to and including order m.

Proof. The order-k term in (C9), for $k \geqslant 2$, is

$$\phi^t_k(x,\mu) = \int_0^t Y_{(k)}\left(\phi^\tau_{(k-1)}(x,\mu),\mu\right)_k d\tau, \tag{C13}$$

where we have considered $\phi^\tau_{(k-1)}$ because Y starts at second order. As $Y_{(k)} = Y_k + Y_{(k-1)}$, and in Y_k only the lower-order terms of $\phi^\tau_{(k-1)}$ contribute to order k,

$$Y_k\left(\phi^\tau_{(k-1)}(x,\mu),\mu\right)_k = Y_k(x,\mu), \tag{C14}$$

because $\phi^t(x,\mu) = x + O(2)$ (C9). Substituting into (C13) we obtain

$$\begin{aligned}\phi^t_k(x,\mu) &= tY_k(x,\mu) + \int_0^t \left(Y_{(k-1)}\left(\phi^\tau_{(k-1)}(x,\mu),\mu\right)\right)_k d\tau \\ &= tY_k(x,\mu) + H_k(x,\mu,t).\end{aligned} \tag{C15}$$

Using $\phi^1_k(x,\mu) = N_k(x,\mu)$ we arrive at the desired result,

$$\phi^1_k(x,\mu) = N_k(x,\mu) = Y_k(x,\mu) + H_k(x,\mu,1).$$

∎

The nonzero terms in $N(x,\mu)$ are

$$\begin{aligned}N_2 &= \begin{pmatrix}\mu_1 + \frac{1}{2}\left(ax_1^2 + bx_2^2\right)\\ -x_1x_2\end{pmatrix},\\ N_3 &= \begin{pmatrix}\mu_2x_1 + \frac{1}{6}cx_1^3 + \frac{1}{2}dx_1x_2^2\\ 0\end{pmatrix}.\end{aligned} \tag{C16}$$

Second-order terms. As $Y_{(1)} = 0$, $H_{(2)} = 0$ and

$$\begin{aligned}Y_2(x,\mu) = N_2(x,\mu) &= \begin{pmatrix}\mu_1 + \frac{1}{2}\left(ax_1^2 + bx_2^2\right)\\ -x_1x_2\end{pmatrix},\\ \phi^t_2(x,\mu) = tY_2(x,\mu) &= \begin{pmatrix}\mu_1t + \frac{1}{2}\left(ax_1^2 + bx_2^2\right)t\\ -x_1x_2t\end{pmatrix}.\end{aligned} \tag{C17}$$

Third-order terms. $Y_{(2)}(x,\mu) = Y_2(x,\mu)$, and

$$\phi^t_{(2)}(x,\mu) = x + \phi^t_2(x,\mu) = \begin{pmatrix} x_1 + \mu_1 t + \frac{1}{2}\left(a x_1^2 + b x_2^2\right)t \\ x_2 - x_1 x_2 t \end{pmatrix},$$

$$Y_{(2)}\left(\phi^t_{(2)}(x,\mu),\mu\right)_3 = \begin{pmatrix} a\mu_1 x_1 t + \frac{1}{2}a^2 x_1^3 t + \frac{1}{2}b(a-2)x_1 x_2^2 t \\ -\mu_1 x_2 t - \frac{1}{2}(a-2)x_1^2 x_2 t - \frac{1}{2}b x_2^3 t \end{pmatrix},$$

$$Y_3(x,\mu) = N_3(x,\mu) - \int_0^1 Y_{(2)}\left(\phi^t_{(2)}(x,\mu),\mu\right)_3 dt = \begin{pmatrix} \left(\mu_2 - \frac{1}{2}a\mu_1\right)x_1 + \left(\frac{1}{6}c - \frac{1}{4}a^2\right)x_1^3 + \left(\frac{1}{2}d + \frac{1}{4}(2-a)b\right)x_1 x_2^2 \\ \frac{1}{2}\mu_1 x_2 - \frac{1}{4}(2-a)x_1^2 x_2 + \frac{1}{4}b x_2^3 \end{pmatrix}.$$

In this way we arrive at the sought ODE up to terms of $O(x^4)$, $O(x^2\mu)$, and $O(\mu^2)$, given in (13).

[1] J. D. Crawford and E. Knobloch, Ann. Rev. Fluid Mech. **23**, 341 (1991).

[2] P. Chossat and G. Iooss, *The Couette-Taylor Problem*, Applied Mathematical Sciences, Vol. 102 (Springer-Verlag, New York, 1994).

[3] B. Eckhardt, T. M. Schneider, B. Hof, and J. Westerweel, Ann. Rev. Fluid Mech. **39**, 447 (2007).

[4] B. Eckhardt, Philos. Trans. R. Soc. A **367**, 449 (2009).

[5] A. P. Willis, P. Cvitanović, and M. Avila, J. Fluid Mech. **721**, 514 (2013).

[6] A. Meseguer and L. N. Trefethen, J. Comput. Phys. **186**, 178 (2003).

[7] H. Faisst and B. Eckhardt, Phys. Rev. Lett. **91**, 224502 (2003).

[8] H. Wedin and R. R. Kerswell, J. Fluid Mech. **508**, 333 (2004).

[9] C. C. T. Pringle and R. R. Kerswell, Phys. Rev. Lett. **99**, 074502 (2007).

[10] C. C. T. Pringle, Y. Duguet, and R. Kerswell, Philos. Trans. R. Soc. A **367**, 457 (2009).

[11] F. Mellibovsky and A. Meseguer, Philos. Trans. R. Soc. A **367**, 545 (2009).

[12] A. de Lozar, F. Mellibovsky, M. Avila, and B. Hof, Phys. Rev. Lett. **108**, 214502 (2012).

[13] Y. Duguet, C. C. T. Pringle, and R. R. Kerswell, Phys. Fluids **20**, 114102 (2008).

[14] F. Mellibovsky and B. Eckhardt, J. Fluid Mech. **709**, 149 (2012).

[15] F. Mellibovsky and B. Eckhardt, J. Fluid Mech. **670**, 96 (2011).

[16] Y. A. Kuznetsov, H. G. E. Meijer, and L. van Veen, Int. J. Bif. Chaos **14**, 2253 (2004).

[17] C. Elphick, E. Tirapegui, M. E. Brachet, P. Coullet, and G. Iooss, Physica D **29**, 95 (1987).

[18] Y. A. Kuznetsov, *Elements of Applied Bifurcation Theory*, 3rd ed. (Springer, Berlin, 2004).

[19] A. Algaba, E. Freire, and E. Gamero, Int. J. Bif. Chaos **8**, 1857 (1998).

[20] J. Murdock, J. Diff. Equ. **205**, 424 (2004).

[21] M. Krupa, SIAM J. Math. Anal. **21**, 1453 (1990).

[22] W. Langford and G. Iooss, in *Bifurcation Problems and Their Numerical Solution*, edited by H. D. Mittelmann and H. Weber, International Series of Numerical Mathematics, Vol. 54 (Birkhäuser, Boston, 1980), pp. 103–134.

[23] J. Guckenheimer and P. Holmes, *Nonlinear Oscillations, Dynamical Systems, and Bifurcations of Vector Fields*, Applied Mathematical Sciences, Vol. 42 (Springer-Verlag, New York, 1983).

[24] J. Sanchez, F. Marques, and J. Lopez, J. Comput. Phys. **180**, 78 (2002).

[25] D. Viswanath, J. Fluid Mech. **580**, 339 (2006).

[26] J. M. Hamilton, J. Kim, and F. Waleffe, J. Fluid Mech. **287**, 317 (1995).

[27] K. Avila, D. Moxey, A. de Lozar, M. Avila, D. Barkley, and B. Hof, Science **333**, 192 (2011).

[28] B. Hof, C. van Doorne, J. Westerweel, F. Nieuwstadt, H. Faisst, B. Eckhardt, H. Wedin, R. Kerswell, and F. Waleffe, Science **305**, 1594 (2004).